Report

Current Biology

Tissue Crowding Induces Caspase-Dependent Competition for Space

Graphical Abstract

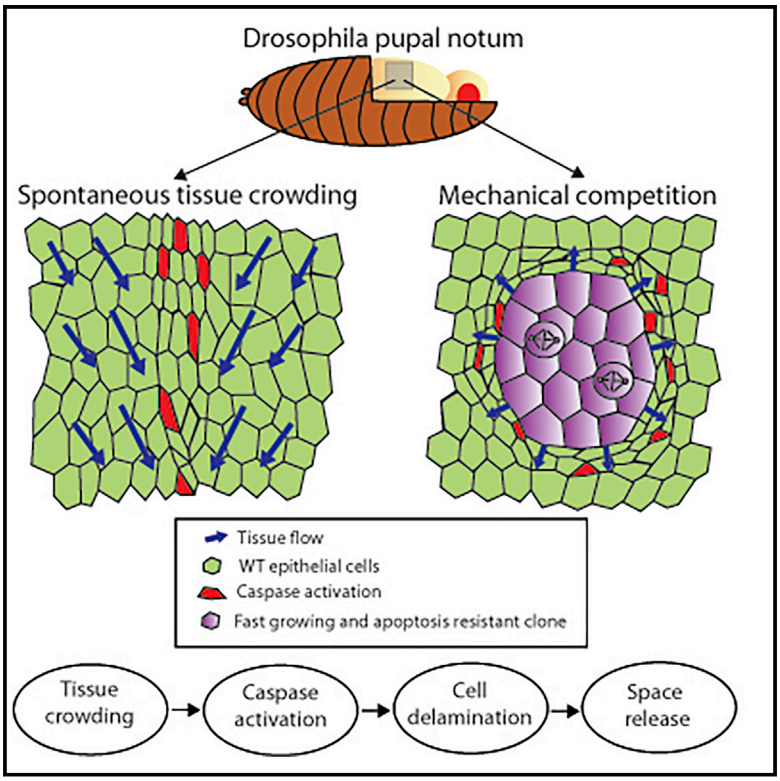

Highlights

- Caspase activation is necessary for cell delamination in the *Drosophila* pupal notum
- Caspase activation is driven by local tissue crowding
- Crowding-induced death is activated near fast-growing clones resistant for apoptosis
- It is a new mode of super-competition that may promote expansion of tumoral cells

Authors

Romain Levayer, Carole Dupont, Eduardo Moreno

Correspondence

eduardo.moreno@research.fchampalimaud.org

In Brief

Using the *Drosophila* pupal notum, Levayer et al. show that epithelium crowding drives random cell elimination through caspase activation and cell delamination. The same phenomenon occurs in the neighborhood of fast growing clones resistant for apoptosis and may promote tumoral cell expansion through the elimination of the neighboring cells.

Levayer et al., 2016, Current Biology *26*, 1–8
March 7, 2016
http://dx.doi.org/10.1016/j.cub.2015.12.072

CellPress

Please cite this article in press as: Levayer et al., Tissue Crowding Induces Caspase-Dependent Competition for Space, Current Biology (2016), http://dx.doi.org/10.1016/j.cub.2015.12.072

Current Biology
Report

Tissue Crowding Induces Caspase-Dependent Competition for Space

Romain Levayer,[1] Carole Dupont,[1] and Eduardo Moreno[1,2,*]
[1]Institute for Cell Biology, University of Bern, Baltzerstrasse 4, 3012 Bern, Switzerland
[2]Champalimaud Centre for the Unknown, 1400-038 Lisbon, Portugal
*Correspondence: eduardo.moreno@research.fchampalimaud.org
http://dx.doi.org/10.1016/j.cub.2015.12.072

SUMMARY

Regulation of tissue size requires fine tuning at the single-cell level of proliferation rate, cell volume, and cell death. Whereas the adjustment of proliferation and growth has been widely studied [1–5], the contribution of cell death and its adjustment to tissue-scale parameters have been so far much less explored. Recently, it was shown that epithelial cells could be eliminated by live-cell delamination in response to an increase of cell density [6]. Cell delamination was supposed to occur independently of caspase activation and was suggested to be based on a gradual and spontaneous disappearance of junctions in the delaminating cells [6]. Studying the elimination of cells in the midline region of the *Drosophila* pupal notum, we found that, contrary to what was suggested before, Caspase 3 activation precedes and is required for cell delamination. Yet, using particle image velocimetry, genetics, and laser-induced perturbations, we confirmed [6] that local tissue crowding is necessary and sufficient to drive cell elimination and that cell elimination is independent of known fitness-dependent competition pathways [7–9]. Accordingly, activation of the oncogene Ras in clones was sufficient to compress the neighboring tissue and eliminate cells up to several cell diameters away from the clones. Mechanical stress has been previously proposed to contribute to cell competition [10, 11]. These results provide the first experimental evidences that crowding-induced death could be an alternative mode of super-competition, namely mechanical super-competition, independent of known fitness markers [7–9], that could promote tumor growth.

RESULTS AND DISCUSSION

We used the *Drosophila* pupal midline to study the process of crowding-induced elimination [6] (Figure 1E). We decided to re-evaluate the contribution of caspase and apoptosis to cell delamination. Inhibition of apoptosis by constitutive overexpression of the apoptosis inhibitor Diap1 almost completely abolishes cell delamination both in the midline and in the rest of the tissue (Figures 1A and 1B; 8-fold reduction; Movies S1A and S1B). This suggested that the contribution of apoptosis/caspase to cell delamination was previously underestimated (only ~30% of delamination was supposed to be caspase dependent) [6]. To confirm that caspase activation is required cell autonomously, we tracked cell delamination events in clones overexpressing Diap1, the baculovirus caspase inhibitor p35, and in clones homozygous for a deletion covering the pro-apoptotic genes *hid*, *grim*, and *reaper*. In every situation, we observed a drastic diminution of proportion of delaminating cells (Figures 1C and 1D; Movies S2A–S2D). Finally, overexpression of Diap1 in the midline using a midline-specific driver (*dad-Gal4*; Figure S1A) led to a 37% increase of the midline width in the adult thorax, in agreement with the expected proportion of cell eliminated (Figures 1B and 1D). Thus, caspase activation is required for cell elimination inside and outside the midline.

Two modes of cell delamination events were described in the midline: apoptosis-induced delamination leading to fast apical area decrease without neighbor exchange and the transient formation of rosettes, or live-cell delamination, where the progressive loss of junctions leads to apical decrease and finally cell delamination (Figure S1B) [6]. We observed a continuum of behavior without clear distinction between the two modes of delamination (Figure S1C). Moreover, we did not observe significant differences in the delamination process occurring in controls nota, the few delamination occurring upon caspase inhibition (*act-gal4, UAS-diap1*) or upon death induction by overexpressing the pro-apoptotic gene *reaper* (Figures S1D and S1E; Movies S1A, S1B, and S1D). This suggested that the different delamination behaviors do not correlate with caspase induction but with other unknown parameters (such as local tissue mechanics and initial cell shape).

Finally, if apoptosis induction is required for cell delamination, Caspase 3 activation should always precede cell delamination. Using two different live reporters of Caspase 3 activity (*UAS-apoliner* [12] and *UAS-scat3* [13]), we systematically observed Caspase 3 activation prior to cell delamination (Figures 2A–2D; Movies S3A and S3C) with a wide range of time delay between initial activation and delamination (from 30 min to >3 hr; Figures 2B and 2D). We concluded that caspase activation precedes and is required for cell delamination.

We next asked what was the cause of apoptosis-induced delamination in the midline. Upregulation/downregulation of growth in the notum are sufficient to upregulate/downregulate

Please cite this article in press as: Levayer et al., Tissue Crowding Induces Caspase-Dependent Competition for Space, Current Biology (2016), http://dx.doi.org/10.1016/j.cub.2015.12.072

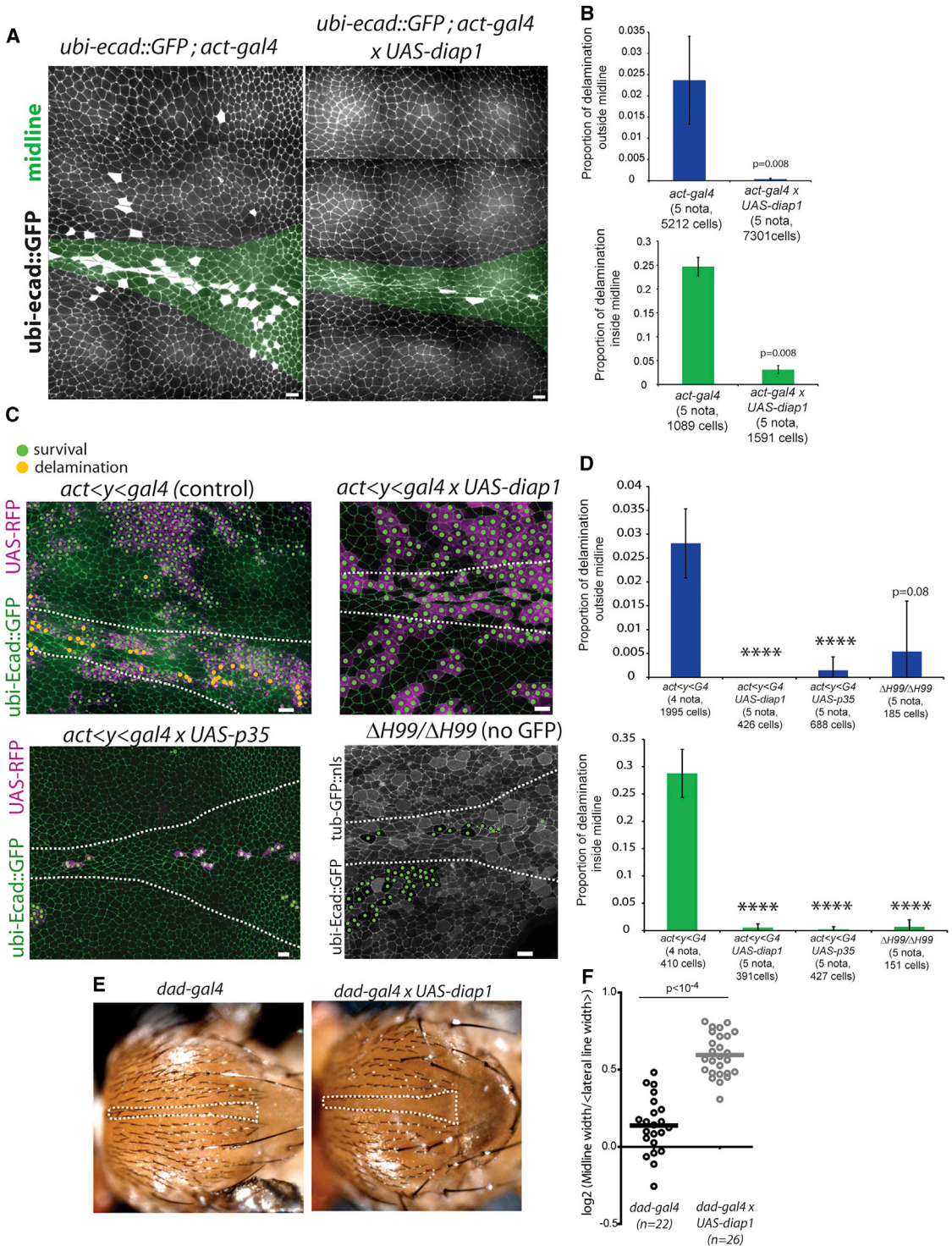

Figure 1. Caspase Activation Is Required for Cell Elimination in the Midline

(A) z projections of E-cad::GFP in live pupal notum in a control (*ubi-Ecad::GFP*; *act-gal4*) or upon ubiquitous inhibition of apoptosis (*ubi-Ecad::GFP*; *act-gal4* × *UAS-diap1*). White cells are cells dying or whose daughter cells are dying over the next 700 min. The midline region is shown in green. The scale bars represent 10 μm.

(B) Proportion of cell undergoing delamination outside the midline (top) and in the midline (bottom). p value, Mann-Whitney test.

(C) z projections of E-cad::GFP in live pupal notum with control clones (*UAS-RFP*; purple; *act<y<G4*), clones overexpressing *diap1* (*UAS-RFP*; purple; *act<y<G4* × *UAS-diap1*), the Caspase 3 inhibitor p35 (*UAS-RFP*; purple; *act<y<G4* × *UAS-p35*), or clones carrying a homozygous deletion covering the three apoptotic genes *hid*, *grim*, and *reaper* (no GFP; *ΔH99/ΔH99*); note that there is also a significant reduction of the delamination rate in the midline in the

(legend continued on next page)

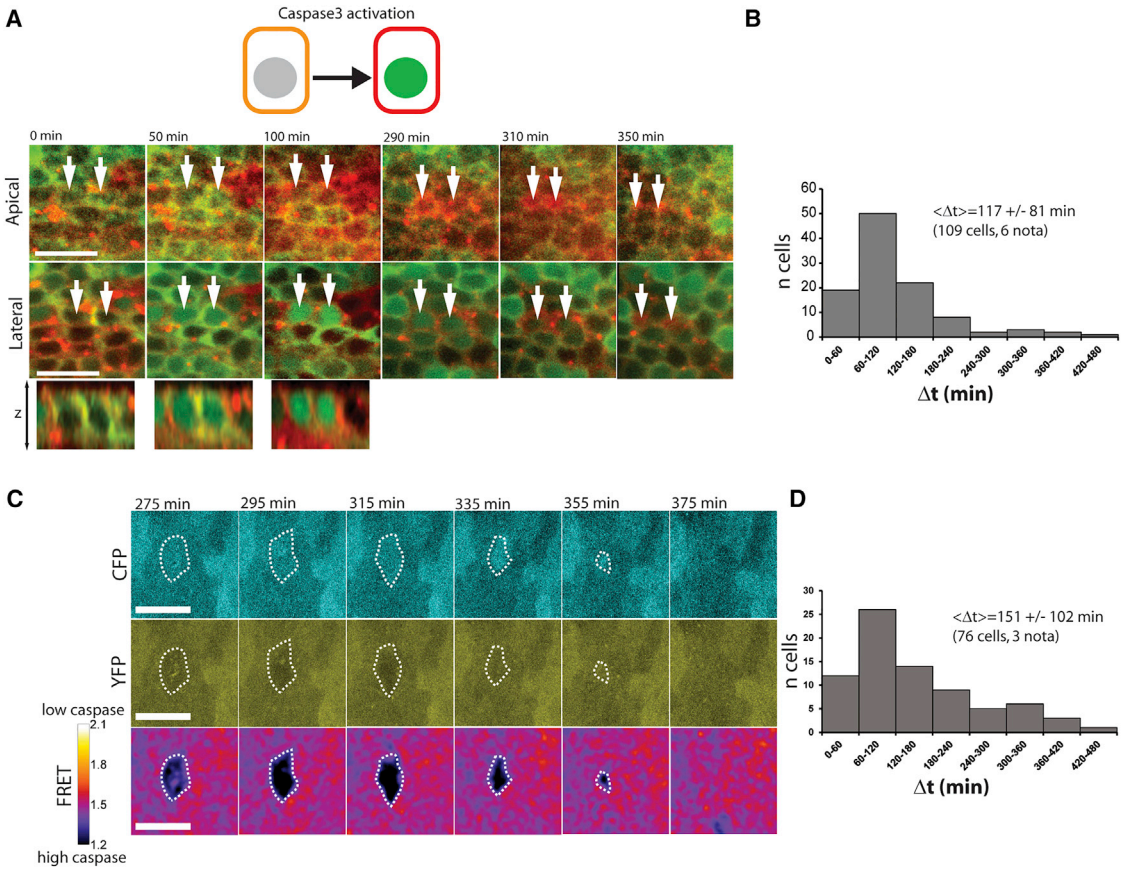

Figure 2. Caspase Activation Precedes Cell Delamination

(A) Snapshots of a movie in the midline of a live pupal notum expressing the caspase sensor *apoliner*. Upon caspase activation, the GFP is relocated to the nucleus, whereas RFP remains at the membrane (top scheme). Apical is the junctional plane showing two cells disappearing (at 350 min; white arrows). Lateral shows the plane containing the nuclei. Note the strong nuclear GFP signal in the two delaminating cells between 50 and 100 min (see sagittal view, bottom). The scale bars represent 10 μm.

(B) Distribution of the lag time between the onset of caspase activation and cell delamination in minutes.

(C) Snapshots of a movie in the midline of a live pupal notum expressing the FRET caspase sensor *scat3*. Upon caspase activation, the FRET signal is reduced. The scale bars represent 10 μm.

(D) Distribution of the lag time between the onset of caspase activation and cell delamination in minutes.

See also Figure S1 and Movie S3.

the rate of cell delamination in the midline [6]. This was suggesting that tissue crowding is responsible for cell delamination. Yet, there was no evidence that mechanical stress can affect cell delamination non-cell-autonomously. Apoptosis in the midline could either be induced cell autonomously and/or regulated by local tissue properties. In the first situation, the delamination rate should not be affected by the behavior of neighboring cells. We observed a significant increase (1.9-fold; $p > 10^{-4}$) of the delamination rate in the WT midline cells when more than 50% of the rest of the midline cells are resistant for apoptosis (*UAS-diap1* clones; Figure 3A). This was suggesting that WT cells can compensate for the absence of delamination in the *UAS-diap1* clones and showed that delamination rate is not only set cell autonomously. Alternatively, cell elimination could be driven by cell competition, a context-dependent apoptosis that eliminates slow-growing cells when neighboring faster-growing cells [11]. However, cell elimination in the midline did not require *flower* or *azot* (Figures S2A and S2B; Movies S2E and S1C),

heterozygous cells (*ΔH99*/+) compared to the WT (0.12 ± 0.02; four nota; 952 cells; $p < 10^{-4}$). The midline is in between the dotted lines. Green spots are surviving cells and orange spots cells dying (or at least one daughter cell dying) after 700 min. The scale bars represent 10 μm.

(D) Proportion of cell undergoing delamination outside the midline (top) and in the midline (bottom). p value, Fisher's exact test. ****$p < 10^{-4}$.

(E) Adult thorax of a control (*dad-gal4*) or upon inhibition of apoptosis in the midline region (*dad-gal4* × *UAS-diap1*). The white dotted lines show the midline region.

(F) Distribution of the log2 of the ratio of width of the midline over the average width of the two adjacent lines of bristles (see the Supplemental Experimental Procedures). One dot, one adult thorax; p value, t test.

See also Figure S1 and Movies S1 and S2.

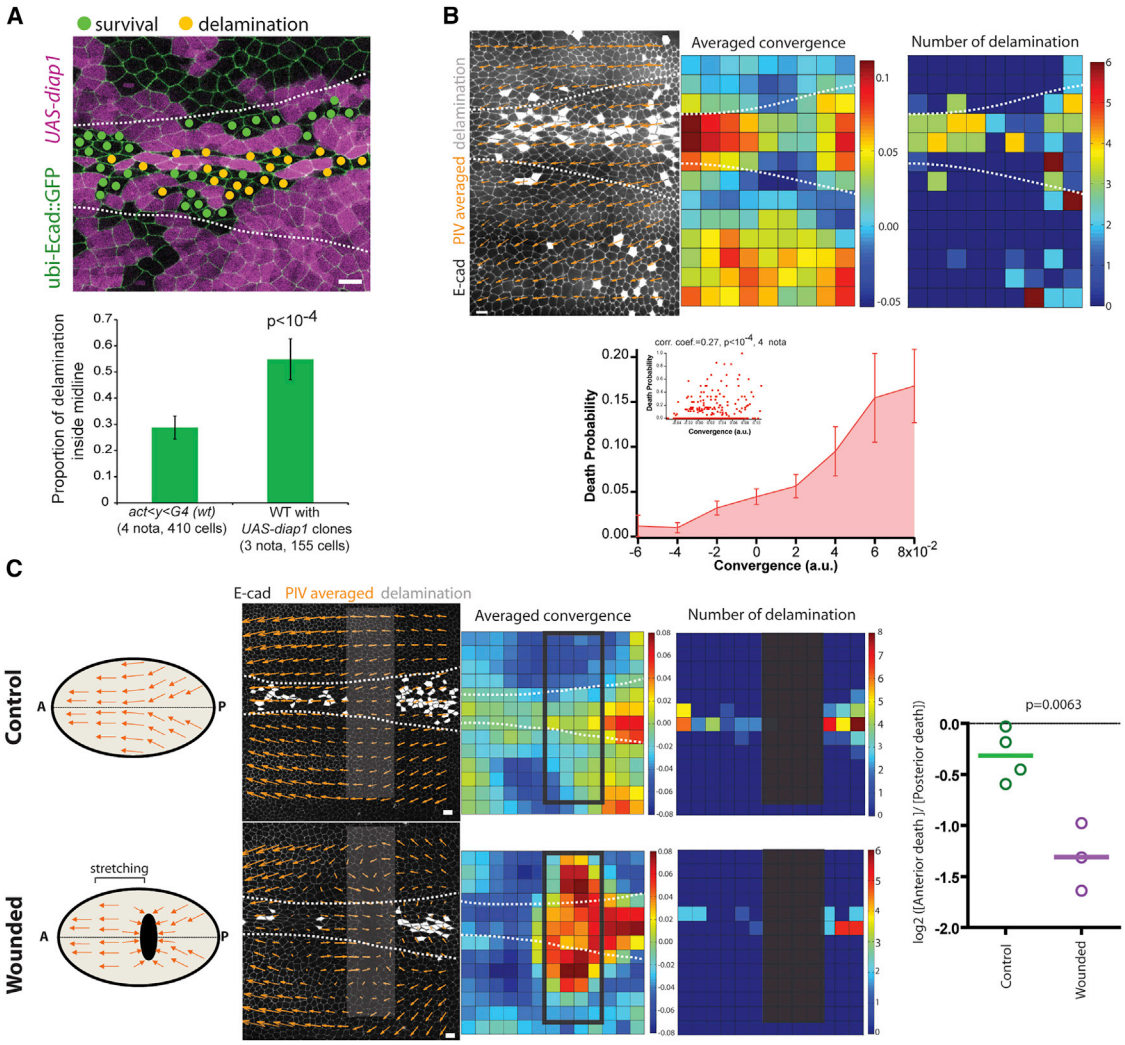

Figure 3. Cell Elimination Is Induced by Local Tissue Crowding

(A) Top: z projections of E-cad::GFP in live pupal notum with clones overexpressing *diap1* (*UAS-RFP*; purple; *act<y<G4* × *UAS-diap1*) covering more than 50% of the midline. The midline is in between the dotted lines. Green spots are surviving WT cells, and orange spots are WT dying cells (or at least one daughter cell dying) after 700 min. The scale bars represent 10 μm. Bottom: proportion of cell undergoing delamination in the midline in a control (act<y<G4; from Figure 1C) or in WT cells in the midline where more than 50% of the cells are overexpressing *diap1*. p value, Fisher's exact test.

(B) Left: averaged PIV vector field (orange) over 700 min on a live pupal notum. White cells are delaminating cells. The midline is in between the dotted lines. Note that this movie is recorded a bit more posterior and lateral compared to the rest of the movies in order to see the high rate of delamination in the lateral-posterior region of the notum (bottom right corner). The scale bar represents 10 μm. Middle: average vector convergence (one notum). Right: local density of cell delamination events. Bottom: binning of the average local death probability against the average local convergence. The inset is the scatterplot from four nota (one dot = one space unit); corr. coef. = 0.27; $p < 10^{-4}$.

(C) Left: scheme of the experiment showing tissue flow (orange) in a control notum (A, anterior; P, posterior; dotted line, midline; tissue flows from the posterior to the anterior side) or upon wound healing after a laser-induced wound (black). Contractions induced by the wound closure generate some stretching on the anterior side, whereas the posterior side is less affected (contractions in the same direction as tissue flow). The corresponding live nota are shown on the right, orange vectors are averaged PIV vectors over 1,000 min, white cells are dying cells, dotted lines are the midline, and the gray rectangle is the zone excluded from the analysis because of the direct damage by the laser. The scale bars represent 10 μm. The local average convergence and the local number of delaminations are shown on the right (one map = one notum); the black rectangles are the zone excluded from the analysis. Right plot: log2 of the ratio of the death probability anterior and posterior to the wound. One dot = one notum. Bars are averages. p value, t test.

See also Figures S2 and S3 and Movies S1, S2, and S4.

two competition-specific genes required for cell elimination [7–9], hence confirming what was previously observed [6]. We therefore tried to confirm that cell delamination was induced by tissue crowding. We used particle image velocimetry (PIV) to quantify local tissue deformations over time [14]. Local tissue crowding is reflected by the positive local convergence of the vector field, which correlates with local increase of cell density and a decrease of cell apical area (see Supplemental Experimental Procedures; Figures 3B, 4A–4C, and S3A; Movie S4A). We observed a significant positive correlation between zones

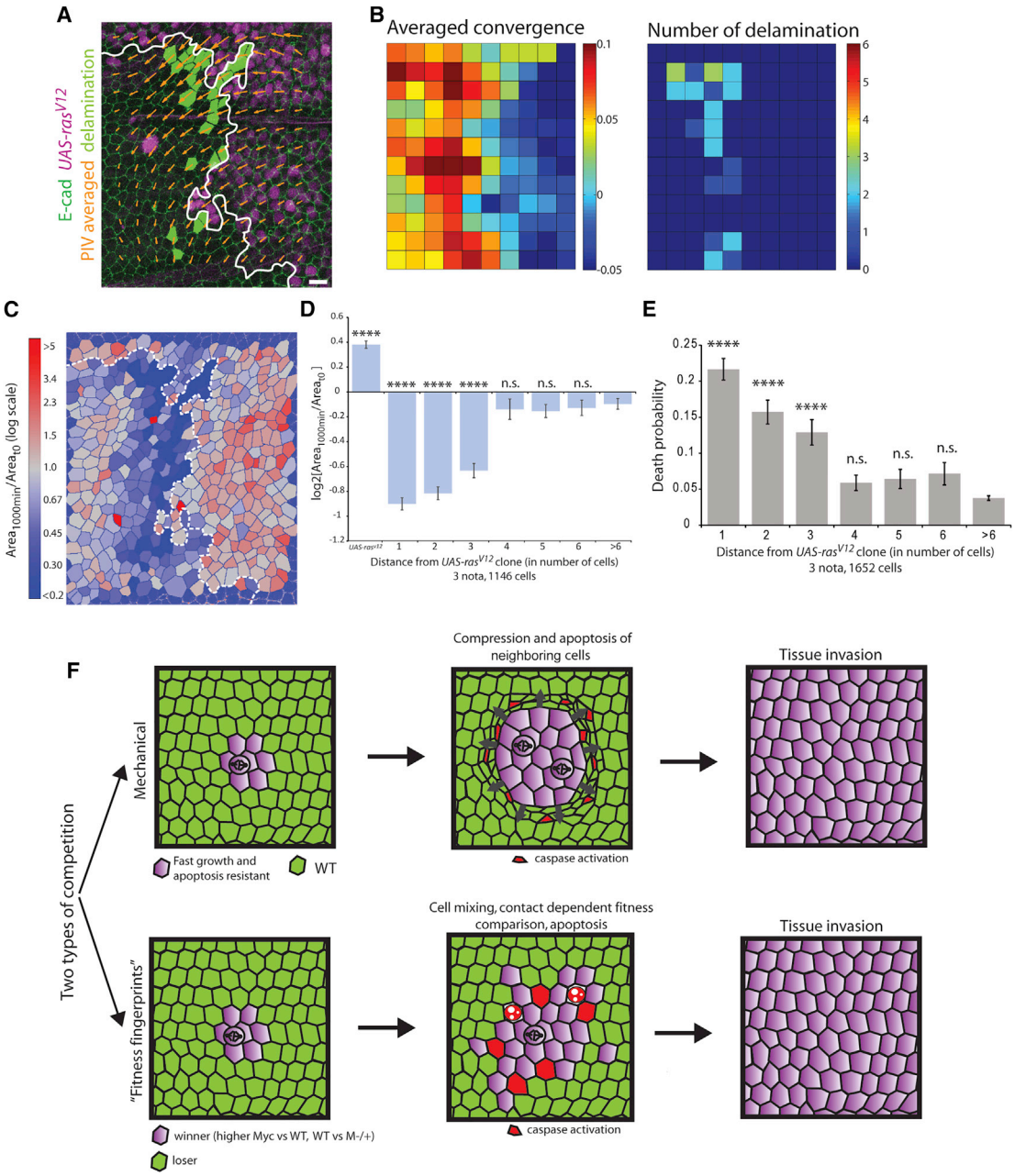

Figure 4. Tissue Crowding Is Sufficient to Induce Cell Elimination

(A) Left: z projection of E-cad::GFP in a live pupal notum with clones overexpressing an activated form of Ras (purple; *hs-flp*;*endo-Ecad*::*GFP*, *gal80ts*; *act<y<G4*, *UAS-nlsRFP* × *UAS-ras^{V12}*). The averaged PIV vectors are in orange (over 1,000 min). Green cells are dying cells. White line, clone contour. The scale bar represents 10 μm.

(B) Left: averaged vector convergence (one notum). Right: local number of cell delamination events.

(C) Fold change of cell apical area (log scale). Dying cells are set to 0 (dark blue); the sum of the area of the daughter cells is used when a cell divides. White dotted line, clone contour.

(D) Log2 of the ratio of the final cell apical area (1,000 min) over the initial apical area in the *UAS-ras^{V12}* clone and in the WT cells (1, touching the clone; >6, more than six cells away from the clone). Dying cells are excluded from this analysis. p values, Mann-Whitney test. n.s., non-significant; ****$p < 10^{-4}$.

(E) Death probability in the WT cells neighboring the *UAS-rasV12* (1, touching the clone; >6, more than six cells away from the clone). p values, Fisher's exact test. n.s., non-significant; ****$p < 10^{-4}$.

(F) Schematic showing the two processes involved in competition: a "fitness fingerprint"-dependent competition (M−/+ and *myc*-dependent competition), where cell elimination is based on a contact-dependent fitness comparison that is enhanced by the high cell mixing between the two populations [9], and mechanical competition, where a clonal population with faster growth and resistant to apoptosis induces crowding in the neighboring WT cells and activates apoptosis. Both processes release space around the clone and allow further growth of the clone.

See also Figures S2 and S4 and Movie S4.

of high convergence and the rate of cell elimination (Figure 3B) both inside the midline and also outside the midline (e.g., in posterior lateral region). Cell delamination could be either the cause or the consequence of local convergence. However, we still observed a positive convergence in the midline and in lateral regions upon inhibition of delamination (*UAS-diap1*; Figure S3B), and delamination occurs on average after a local peak of convergence (Figure S3C). Thus, cell delamination is more likely to be the consequence of tissue convergence. To check whether local crowding is necessary to induce delamination, we perturb the posterior to anterior tissue flow by wounding the notum by laser exposure (Figure 3C, left scheme). The local contraction induced by wound healing will produce a local stretching of the tissue on the anterior side of the wound, whereas the posterior side should be less affected (Figure 3C). Accordingly, we observed a strong reduction of convergence flow anterior to the wound (Figure 3C, middle panels; Movie S4B), leading to a local reduction of the rate of delamination in the midline (Figure 3C, middle and right panels). This effect is unlikely to be driven by some pro-survival diffusive factors, which should affect equally the anterior and posterior side of the wound. Therefore, we concluded that local tissue convergence is necessary to induce delamination in the midline.

We then tried to induce ectopic tissue crowding. Inducing rapid cell growth in clones should produce compressive forces both within the clone and in the neighboring tissue [10]. If apoptosis is also blocked in the clone, our results predict that cell delamination should occur preferentially outside the clone. We induced rapid growth and survival through conditional expression in clones of an active allele of the oncogene *ras* (*UAS-ras^{V12}*) [15–17]. Activation over 16 hr was sufficient to observe a significant expansion of the *UAS-rasV12* clones and an increase of apical cell area (40%) as well as the compaction of the neighboring WT cells, as outlined by the local convergence in the vector field (Movie S4C; Figures 4A and 4B) and the local decrease of apical cell area (Figures 4C and 4D). This was sufficient to produce ectopic cell delamination up to three cell diameters away from the *ras^{V12}* clones (Movie S4C; Figures 4A, 4B, and 4E), in agreement with the regions where cells undergo significant reduction of their apical area (Figure 4D). These delaminations were not driven by fitness-dependent competition as they are not strictly contact dependent [7, 9, 18], and we could not detect any induction of the fitness marker *fwe^{lose}* [7, 9] in the cells neighboring the clones (Figure S2C). Altogether, we concluded that ectopic tissue crowding is sufficient to drive cell elimination.

Tissue crowding was previously suggested to induce live-cell delamination, which preceded caspase activation [6]. Using the midline region of the *Drosophila* pupal notum, we confirmed that local tissue crowding is necessary and sufficient to drive cell delamination and that this process is independent of the fitness-dependent competition pathway [6]. We showed, however, that caspase activation precedes and is necessary for cell delamination in the midline. This discrepancy may rely on the different drivers used to block apoptosis (*pnr-gal4* in [6]; *act-gal4* and homozygous mutants in this study), which may only block partially caspase activation with lower levels of induction. Our results are not incompatible with a live-cell delamination process as caspase may also prime the cells for delamination prior to apoptosis induction. Accordingly, we observed several cases of transient caspase activation that are not followed by delamination (Figure S1F; Movie S3B). This may also suggest that high and sustained stress is required to reach the high levels of caspase activation necessary for delamination and apoptosis termination. Our results also suggest that one (or several) yet unknown pathway(s) can detect local tissue crowding, activate caspase, and the subsequent cell delamination. Interestingly, preliminary results suggest that the most obvious candidates are not involved, including the JNK pathway [19, 20], p53, and the Hippo pathway [21] (Figure S4, as reported in [6]), although we cannot exclude some redundancy between these pathways. This new and uncharacterized pathway could play a critical role for size regulation and cell elimination in several developmental contexts such as cell elimination in the crowded central region of wing imaginal disc [22, 23] and elimination of amnioserosa cells during dorsal closure [24], of larval cells in the pupal abdomen [25], in the folds of the pupal legs [26], or during rotation of the genitalia [27]. Confrontation of two cell populations with different growth rate can generate local mechanical stress [10]. More precisely, the fast-growing population and the neighboring cells should experience compressive stress. In the framework of spontaneous and caspase-independent cell delamination, cell elimination would mostly take place within the fast-growing clone and act as a tumor suppressor mechanism. Interestingly, several pathways promoting growth also inhibit apoptosis and are involved in cancer progression [28]. In such conditions, our results suggest, however, that cell elimination would be blocked in the fast-growing clone and occur preferentially in the neighboring cells, as observed upon Ras activation. In that situation, crowding-induced elimination would facilitate the expansion of the fast-growing clone and could promote tumor expansion (Figure 4F). The resistance to apoptosis induced by Ras [16, 29] is probably critical for this process as strong overexpression of *myc* (a regulator of growth downstream of Ras) [17] in clones increases cell death within the clone (Figure S4E; Movie S2F; see also [30, 31]) and does not produce any obvious deformations in the neighboring tissue (Movie S2F). Moreover, Ras clones undergo cell sorting and form smooth boundaries [32], whereas mild differences in *myc* expression increase cell mixing and cell-cell intercalation [9], which should dissipate mechanical stress. Therefore, crowding-induced death is unlikely to participate in *myc*-dependent competition. So far, super-competition was defined as the active elimination of WT cells by faster-proliferating cells [11, 33, 34] through the local comparison of fitness. This is based on "fitness fingerprints," such as the transmembrane protein Flower [7, 9, 35], which are used to compare fitness state not only in cell competition but also in post-mitotic neurons [8, 35, 36]. Alternatively, mechanical stress was also previously suggested to participate in cell competition [10, 11]. Here, we provide for the first time evidences that mechanical stress could indeed be involved in an alternative mode of competition, namely mechanical super-competition, which eliminates neighboring cells randomly through

crowding without prior selection and fitness comparison [7–9] (Figure 4F).

SUPPLEMENTAL INFORMATION

Supplemental Information includes Supplemental Experimental Procedures, four figures, and four movies and can be found with this article online at http://dx.doi.org/10.1016/j.cub.2015.12.072.

AUTHOR CONTRIBUTIONS

R.L. and E.M. designed the experiments. R.L. performed and analyzed the experiments. C.D. did the experiments shown in Figure S4, and R.L. and E.M. wrote the manuscript.

ACKNOWLEDGMENTS

We would like to thank members of the E.M. lab for critical reading of this manuscript. We are also very grateful to A. Bergmann, M. Gonzalez-Gaitan, M. KangoSingh, M. Miura, B.J. Thompson, the Bloomington stock center, the Kyoto Drosophila Genomics and Genetics Resources, the Vienna Drosophila Resource Center, and the DSHB (Developmental Studies Hybridoma Bank) for sharing stocks and reagents and to B. Aigouy for the Packing Analyzer. R.L. was supported by a Human Frontier post-doctoral fellowship (LT000178/2013). Work in our laboratory is funded by the European Research Council, Swiss National Science Foundation, Josef Steiner Cancer Research Foundation, and the Swiss Cancer League.

Received: October 13, 2015
Revised: November 25, 2015
Accepted: December 31, 2015
Published: February 18, 2016

REFERENCES

1. Andersen, D.S., Colombani, J., and Léopold, P. (2013). Coordination of organ growth: principles and outstanding questions from the world of insects. Trends Cell Biol. *23*, 336–344.
2. McClatchey, A.I., and Yap, A.S. (2012). Contact inhibition (of proliferation) redux. Curr. Opin. Cell Biol. *24*, 685–694.
3. Hufnagel, L., Teleman, A.A., Rouault, H., Cohen, S.M., and Shraiman, B.I. (2007). On the mechanism of wing size determination in fly development. Proc. Natl. Acad. Sci. USA *104*, 3835–3840.
4. Streichan, S.J., Hoerner, C.R., Schneidt, T., Holzer, D., and Hufnagel, L. (2014). Spatial constraints control cell proliferation in tissues. Proc. Natl. Acad. Sci. USA *111*, 5586–5591.
5. Delarue, M., Montel, F., Vignjevic, D., Prost, J., Joanny, J.F., and Cappello, G. (2014). Compressive stress inhibits proliferation in tumor spheroids through a volume limitation. Biophys. J. *107*, 1821–1828.
6. Marinari, E., Mehonic, A., Curran, S., Gale, J., Duke, T., and Baum, B. (2012). Live-cell delamination counterbalances epithelial growth to limit tissue overcrowding. Nature *484*, 542–545.
7. Rhiner, C., López-Gay, J.M., Soldini, D., Casas-Tinto, S., Martín, F.A., Lombardía, L., and Moreno, E. (2010). Flower forms an extracellular code that reveals the fitness of a cell to its neighbors in Drosophila. Dev. Cell *18*, 985–998.
8. Merino, M.M., Rhiner, C., Lopez-Gay, J.M., Buechel, D., Hauert, B., and Moreno, E. (2015). Elimination of unfit cells maintains tissue health and prolongs lifespan. Cell *160*, 461–476.
9. Levayer, R., Hauert, B., and Moreno, E. (2015). Cell mixing induced by myc is required for competitive tissue invasion and destruction. Nature *524*, 476–480.
10. Shraiman, B.I. (2005). Mechanical feedback as a possible regulator of tissue growth. Proc. Natl. Acad. Sci. USA *102*, 3318–3323.
11. Vincent, J.P., Fletcher, A.G., and Baena-Lopez, L.A. (2013). Mechanisms and mechanics of cell competition in epithelia. Nat. Rev. Mol. Cell Biol. *14*, 581–591.
12. Bardet, P.L., Kolahgar, G., Mynett, A., Miguel-Aliaga, I., Briscoe, J., Meier, P., and Vincent, J.P. (2008). A fluorescent reporter of caspase activity for live imaging. Proc. Natl. Acad. Sci. USA *105*, 13901–13905.
13. Takemoto, K., Nagai, T., Miyawaki, A., and Miura, M. (2003). Spatio-temporal activation of caspase revealed by indicator that is insensitive to environmental effects. J. Cell Biol. *160*, 235–243.
14. Bosveld, F., Bonnet, I., Guirao, B., Tlili, S., Wang, Z., Petitalot, A., Marchand, R., Bardet, P.L., Marcq, P., Graner, F., and Bellaïche, Y. (2012). Mechanical control of morphogenesis by Fat/Dachsous/Four-jointed planar cell polarity pathway. Science *336*, 724–727.
15. Fortini, M.E., Simon, M.A., and Rubin, G.M. (1992). Signalling by the sevenless protein tyrosine kinase is mimicked by Ras1 activation. Nature *355*, 559–561.
16. Bergmann, A., Agapite, J., McCall, K., and Steller, H. (1998). The Drosophila gene hid is a direct molecular target of Ras-dependent survival signaling. Cell *95*, 331–341.
17. Prober, D.A., and Edgar, B.A. (2000). Ras1 promotes cellular growth in the Drosophila wing. Cell *100*, 435–446.
18. Simpson, P., and Morata, G. (1981). Differential mitotic rates and patterns of growth in compartments in the Drosophila wing. Dev. Biol. *85*, 299–308.
19. Pereira, A.M., Tudor, C., Kanger, J.S., Subramaniam, V., and Martin-Blanco, E. (2011). Integrin-dependent activation of the JNK signaling pathway by mechanical stress. PLoS ONE *6*, e26182.
20. Martin-Blanco, E., Pastor-Pareja, J.C., and Garcia-Bellido, A. (2000). JNK and decapentaplegic signaling control adhesiveness and cytoskeleton dynamics during thorax closure in Drosophila. Proc. Natl. Acad. Sci. USA *97*, 7888–7893.
21. Schroeder, M.C., and Halder, G. (2012). Regulation of the Hippo pathway by cell architecture and mechanical signals. Semin. Cell Dev. Biol. *23*, 803–811.
22. Legoff, L., Rouault, H., and Lecuit, T. (2013). A global pattern of mechanical stress polarizes cell divisions and cell shape in the growing Drosophila wing disc. Development *140*, 4051–4059.
23. Mao, Y., Tournier, A.L., Hoppe, A., Kester, L., Thompson, B.J., and Tapon, N. (2013). Differential proliferation rates generate patterns of mechanical tension that orient tissue growth. EMBO J. *32*, 2790–2803.
24. Solon, J., Kaya-Copur, A., Colombelli, J., and Brunner, D. (2009). Pulsed forces timed by a ratchet-like mechanism drive directed tissue movement during dorsal closure. Cell *137*, 1331–1342.
25. Ninov, N., Menezes-Cabral, S., Prat-Rojo, C., Manjón, C., Weiss, A., Pyrowolakis, G., Affolter, M., and Martín-Blanco, E. (2010). Dpp signaling directs cell motility and invasiveness during epithelial morphogenesis. Curr. Biol. *20*, 513–520.
26. Monier, B., Gettings, M., Gay, G., Mangeat, T., Schott, S., Guarner, A., and Suzanne, M. (2015). Apico-basal forces exerted by apoptotic cells drive epithelium folding. Nature *518*, 245–248.
27. Suzanne, M., Petzoldt, A.G., Spéder, P., Coutelis, J.B., Steller, H., and Noselli, S. (2010). Coupling of apoptosis and L/R patterning controls stepwise organ looping. Curr. Biol. *20*, 1773–1778.
28. O'Hayre, M., Degese, M.S., and Gutkind, J.S. (2014). Novel insights into G protein and G protein-coupled receptor signaling in cancer. Curr. Opin. Cell Biol. *27*, 126–135.
29. Kurada, P., and White, K. (1998). Ras promotes cell survival in Drosophila by downregulating hid expression. Cell *95*, 319–329.
30. Montero, L., Müller, N., and Gallant, P. (2008). Induction of apoptosis by Drosophila Myc. Genesis *46*, 104–111.
31. Zhang, C., Casas-Tintó, S., Li, G., Lin, N., Chung, M., Moreno, E., Moberg, K.H., and Zhou, L. (2015). An intergenic regulatory region mediates

Drosophila Myc-induced apoptosis and blocks tissue hyperplasia. Oncogene *34*, 2385–2397.

32. Prober, D.A., and Edgar, B.A. (2002). Interactions between Ras1, dMyc, and dPI3K signaling in the developing Drosophila wing. Genes Dev. *16*, 2286–2299.
33. de la Cova, C., Abril, M., Bellosta, P., Gallant, P., and Johnston, L.A. (2004). Drosophila myc regulates organ size by inducing cell competition. Cell *117*, 107–116.
34. Moreno, E., and Basler, K. (2004). dMyc transforms cells into super-competitors. Cell *117*, 117–129.
35. Merino, M.M., Rhiner, C., Portela, M., and Moreno, E. (2013). "Fitness fingerprints" mediate physiological culling of unwanted neurons in Drosophila. Curr. Biol. *23*, 1300–1309.
36. Moreno, E., Fernandez-Marrero, Y., Meyer, P., and Rhiner, C. (2015). Brain regeneration in Drosophila involves comparison of neuronal fitness. Curr. Biol. *25*, 955–963.

Current Biology, Volume *26*

Supplemental Information

Tissue Crowding Induces Caspase-Dependent Competition for Space

Romain Levayer, Carole Dupont, and Eduardo Moreno

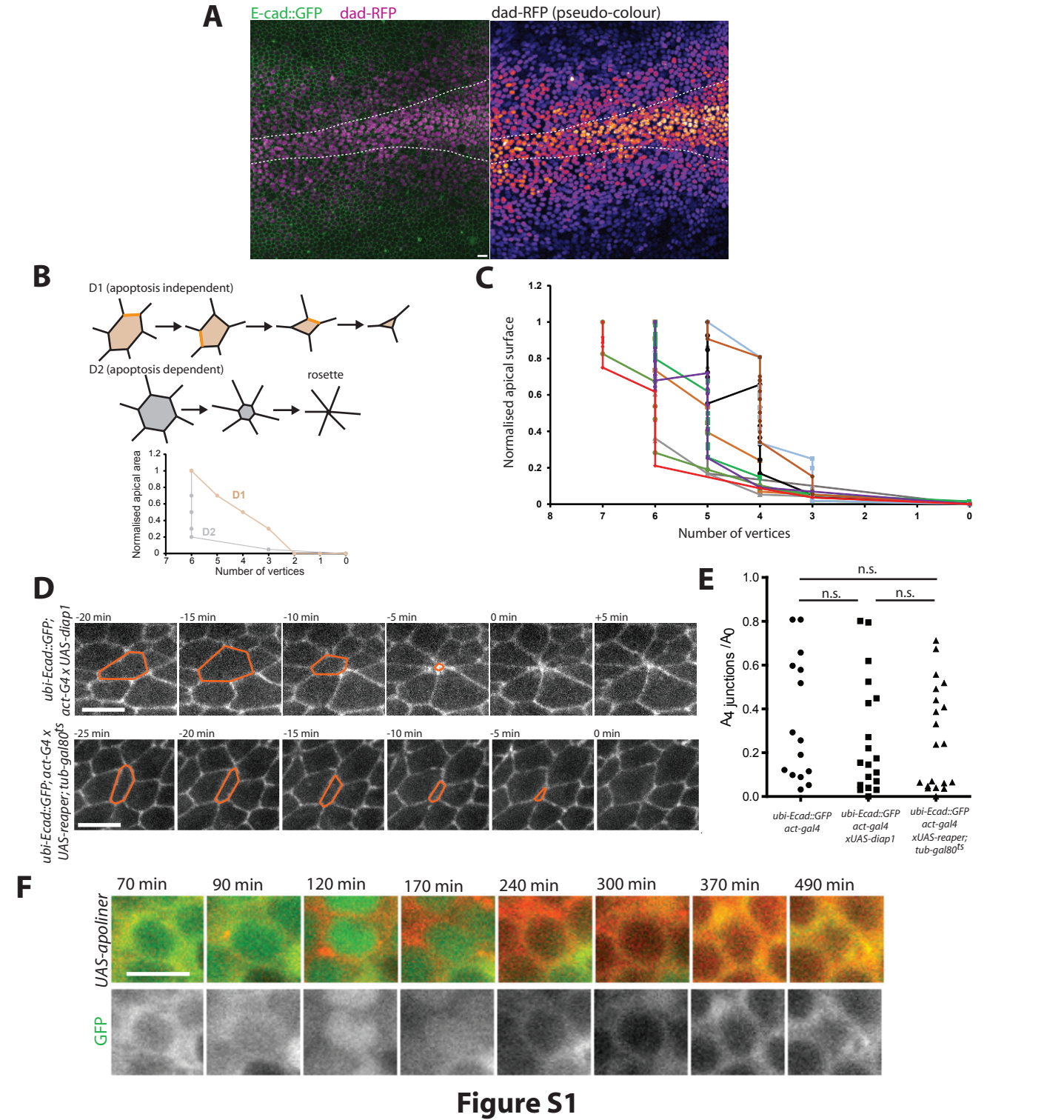
A
E-cad::GFP
dad-RFP
dad-RFP (pseudo-colour)
B
D1 (apoptosis independent)
D2 (apoptosis dependent)
rosette
Normalised apical area
D1
D2
Number of vertices
C
Normalised apical surface
Number of vertices
D
ubi-Ecad::GFP; act-G4 x UAS-diap1
-20 min
-15 min
-10 min
-5 min
0 min
+5 min
ubi-Ecad::GFP; act-G4 x UAS-reaper; tub-gal80ts
-25 min
-20 min
-15 min
-10 min
-5 min
0 min
E
n.s.
n.s.
n.s.
A4 junctions /A0
ubi-Ecad::GFP act-gal4
ubi-Ecad::GFP act-gal4 xUAS-diap1
ubi-Ecad::GFP act-gal4 xUAS-reaper; tub-gal80ts
F
70 min
90 min
120 min
170 min
240 min
300 min
370 min
490 min
UAS-apoliner
GFP

Figure S1

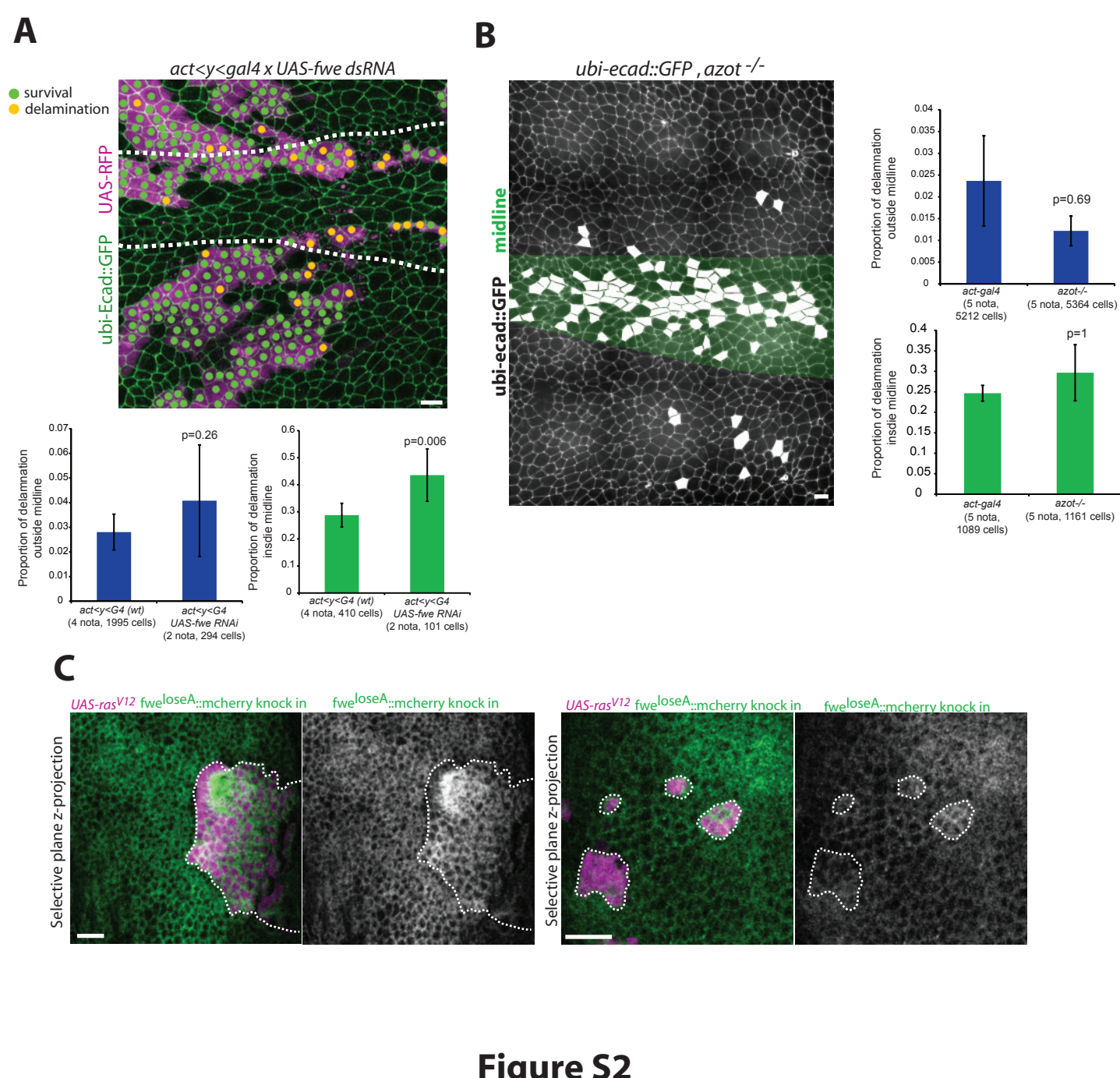
A
act<y<gal4 x UAS-fwe dsRNA
survival
delamination
UAS-RFP
ubi-Ecad::GFP
Proportion of delamnation outside midline
p=0.26
act<y<G4 (wt) (4 nota, 1995 cells)
act<y<G4 UAS-fwe RNAi (2 nota, 294 cells)
Proportion of delamnation insdie midline
p=0.006
act<y<G4 (wt) (4 nota, 410 cells)
act<y<G4 UAS-fwe RNAi (2 nota, 101 cells)
B
ubi-ecad::GFP , azot -/-
midline
ubi-ecad::GFP
Proportion of delamnation outside midline
p=0.69
act-gal4 (5 nota, 5212 cells)
azot-/- (5 nota, 5364 cells)
Proportion of delamnation insdie midline
p=1
act-gal4 (5 nota, 1089 cells)
azot-/- (5 nota, 1161 cells)
C
UAS-rasV12 fweloseA::mcherry knock in
fweloseA::mcherry knock in
Selective plane z-projection
UAS-rasV12 fweloseA::mcherry knock in
fweloseA::mcherry knock in
Selective plane z-projection

Figure S2

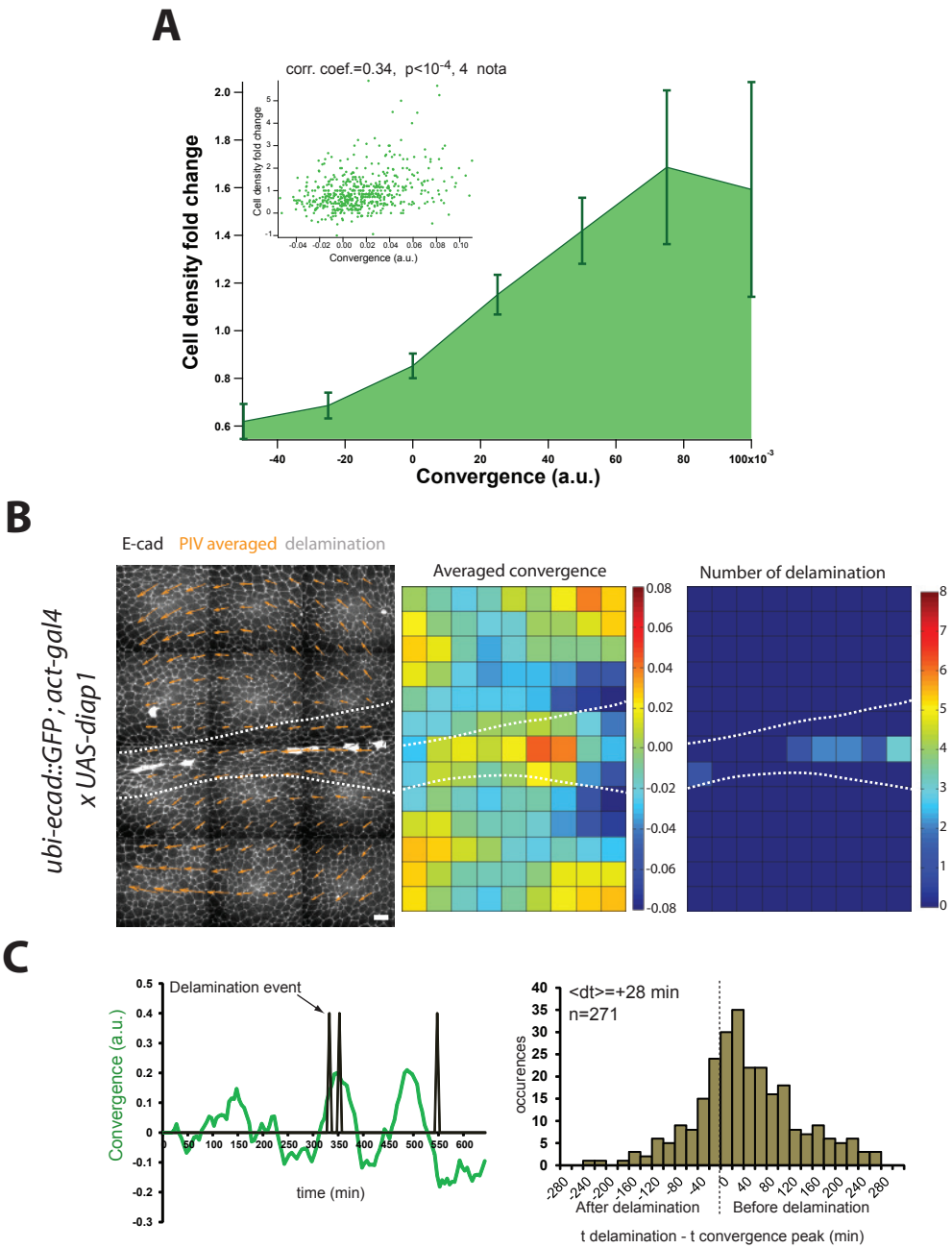
A
corr. coef.=0.34, p<10-4, 4 nota
Cell density fold change
Convergence (a.u.)
B
E-cad PIV averaged delamination
ubi-ecad::GFP ; act-gal4
x UAS-diap1
Averaged convergence
Number of delamination
C
Delamination event
Convergence (a.u.)
time (min)
<dt>=+28 min
n=271
occurences
After delamination
Before delamination
t delamination - t convergence peak (min)

Figure S3

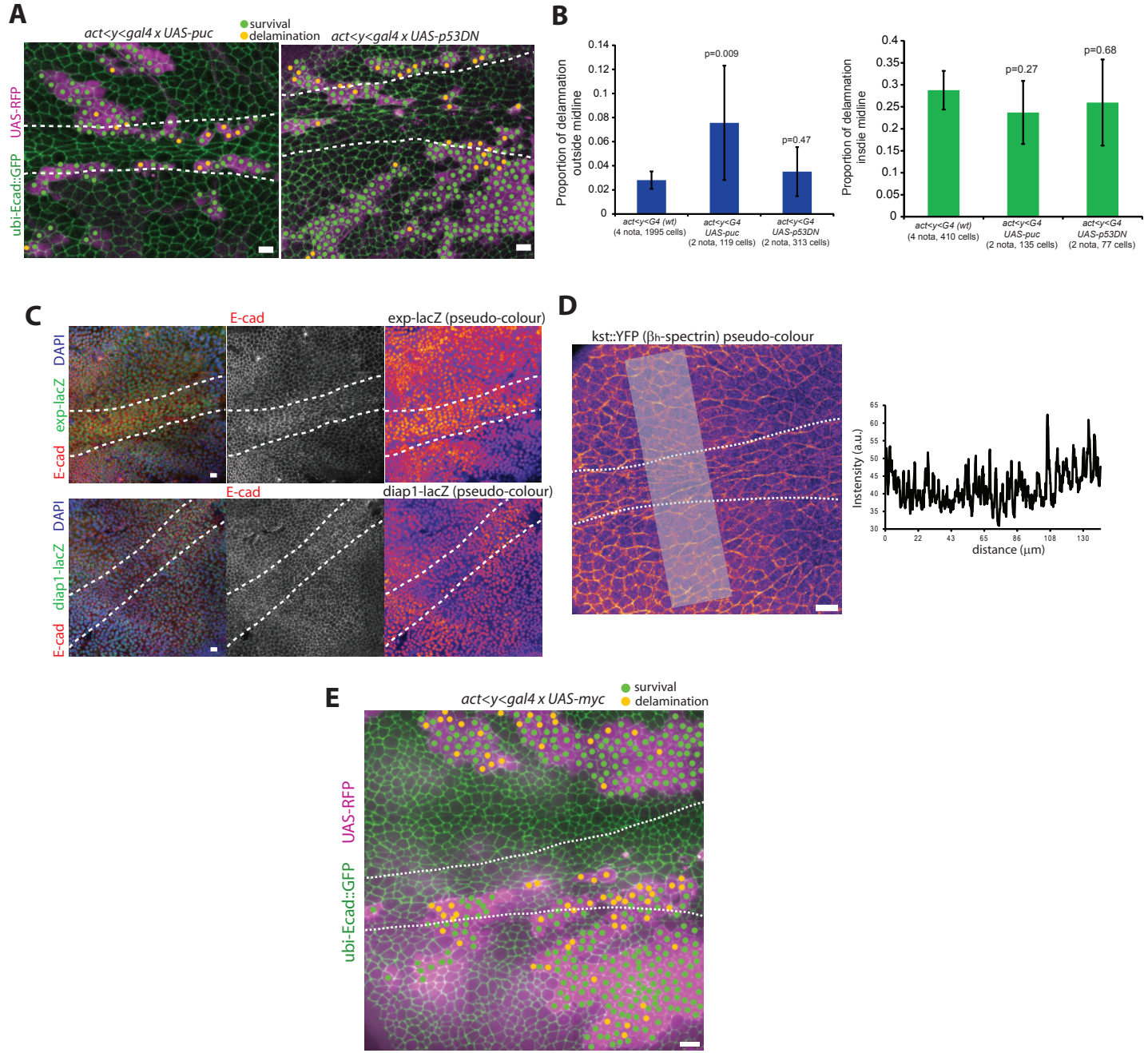
A
act<y<gal4 x UAS-puc
survival
delamination
act<y<gal4 x UAS-p53DN
UAS-RFP
ubi-Ecad::GFP
B
Proportion of delamnation outside midline
0.14
0.12
0.1
0.08
0.06
0.04
0.02
0
p=0.009
p=0.47
act<y<G4 (wt)
(4 nota, 1995 cells)
act<y<G4
UAS-puc
(2 nota, 119 cells)
act<y<G4
UAS-p53DN
(2 nota, 313 cells)
Proportion of delamnation insdie midline
0.4
0.35
0.3
0.25
0.2
0.15
0.1
0.05
0
p=0.27
p=0.68
act<y<G4 (wt)
(4 nota, 410 cells)
act<y<G4
UAS-puc
(2 nota, 135 cells)
act<y<G4
UAS-p53DN
(2 nota, 77 cells)
C
E-cad
exp-lacZ (pseudo-colour)
DAPI
exp-lacZ
E-cad
E-cad
diap1-lacZ (pseudo-colour)
DAPI
diap1-lacZ
E-cad
D
kst::YFP (βh-spectrin) pseudo-colour
Instensity (a.u.)
65
60
55
50
45
40
35
30
0
22
43
65
86
108
130
distance (μm)
E
act<y<gal4 x UAS-myc
survival
delamination
UAS-RFP
ubi-Ecad::GFP

Figure S4

Supplemental information

Supplemental figure legends

Figure S1: There is a continuum of delamination behaviours (related to Fig. 1 and Fig. 2)

A: Left, z-projection of E-cad::GFP (green) and the reporter of Dpp pathway *dad-RFP* (magenta and pseudo-colour) in a live pupal notum. White dotted line=midline. Scale bars=10μm. **B:** Top, Schematic of the two types of delamination described in [S1], D1 delaminations were described as apoptotic independent delaminations where junctions gradually disappear leading to gradual decrease of apical surface (bottom graph, pink curve), D2 delaminations were described as apoptotic dependent delaminations where apical surface shrink rapidly without junction loss, leading to a transitory rosette figure (bottom graph, grey curve) **C:** Evolution of the normalised apical surface and number of vertices in different examples of delamination occurring in the midline of WT nota. Note the great diversity of behaviours without clear distinction between two behaviours. **D:** Top, example of a D2 type delamination event in the midline despite inhibition of apoptosis (*ubi-Ecad::GFP; act-G4 x UAS-diap1*), Bottom, example of a D1 type delamination event outside the midline upon induction of apoptosis by the pro-apoptotic gene *reaper* (*ubi-Ecad::GFP; act-G4 x UAS-reaper; tub-gal80^{ts}*). **E:** Ratio of the apical area when cells have 4 junctions left over the initial apical area in the midline of a control notum (*ubi-Ecad::GFP; act-G4*), in the midline upon inhibition of apoptosis (*ubi-Ecad::GFP; act-G4 x UAS-diap1*), outside the midline upon induction of apoptosis (*ubi-Ecad::GFP; act-G4 x UAS-reaper, tub-gal80^{ts}*). One dot/square/triangle= one delamination event. n.s.= Non Significant, P-values=Mann Whitney test. **F:** Example of a cell undergoing transient caspase activation (visualised with *UAS-apoliner*). Note that the GFP produced after the peak of caspase activation (t=120min) is located at the membrane, indicating the absence of caspase activity. Scale bar = 5μm.

Figure S2: Crowding induced delamination is not induced by classical competition genes (related to Fig. 3 and Fig. 4)

A: Top, z-projection of E-cad::GFP in a live pupal notum with clones overexpressing *fwe-dsRNA* (*UAS-RFP*, purple, *act<y<G4 x UAS-fwe RNAi*). The midline is in between the dotted lines. Green spots are surviving cells and orange spots dying cells (or at least one daughter cell dying) after 700 minutes. Scale bars=10μm. Bottom, Proportion of cell undergoing delamination outside the midline (top) and in the midline (bottom). Controls (*act<y<G4*) come from Fig. 1C,D. Error bars are 95% confidence intervals. P-values=Fisher exact test. **B:** Left, z-projections of E-cad::GFP in a live pupal homozygous mutant for the competition gene *azot*. White cells are cells dying or whose daughter cells are dying over the next 700min. The midline region is shown in green. Scale bar=10μm. Right, proportion of cells undergoing delamination outside the midline (top) and in the midline (bottom). Controls (*act-gal4*) come from Fig. 1A,B. Error bars=s.e.m.. P-values=Man-Whitney test. **C:** Two examples of selective plane projection of a knock-in fusion of the competition marker *fwe^{loseA}* (fwe^{loseA}::mcherry knock in) in live wing imaginal disc with clones overexpressing an activated form of Ras (*UAS-ras^{V12}*). There is no increase of *fwe^{loseA}* in the cells neighbouring the clones. White dotted lines=clone contours. Scale bars=10μm

Figure S3: Convergent flow is not induced by cell delamination (related to Fig. 3)

A: Binning of the average local cell density fold change against the average local convergence determined by PIV in WT pupal nota (see **Fig. 3B**). The inset is the scatter plot from 4 nota (1 dot=1 space unit), corr. coef. =0.34, $p<10^{-4}$. This correlation shows that convergence cannot be only driven by delamination and replacement of the dying cells, which would lead to no change in the local cell density. **B:** Left, averaged PIV vector field (orange) over 700min on a live pupal notum expressing the apoptosis inhibitor *diap1* (one notum). White cells are delaminating cells. The midline is between the dotted lines. Scale bar=10μm. Middle, Average vector convergence. Right, local number of cell delamination events. Note that there is still a significant convergence in the midline and in the lateral regions despite the strong inhibition/absence of delamination. **C:** Left, example of a time course of the local convergence (green curve) in one unit of space (see experimental procedures) and the local delamination events (black peaks) from a WT live pupal notum. Right, distribution of the lag-time between a delamination event and the closest peak of convergence (see experimental procedures). The average is +28 min (n=271 delamination events), suggesting that on average delamination occurs after a local peak of convergence.

Figure S4: Cell delamination in the midline is not driven by JNK, p53 or the Hippo pathway (related to Fig. 4)

A: z-projection of E-cad::GFP in a live pupal notum with clones overexpressing the phosphatase Puckered, a negative regulator of JNK pathway (*UAS-puc*, purple, *act<y<G4 x UAS-puc*), or a dominant negative allele of p53 (*UAS-p53DN*, purple, *act<y<G4 x UAS-p53DN*). The midline is in between the dotted lines. Green spots are

surviving cells and orange spots dying cells (or at least one daughter cell dying) after 700 minutes. Scale bars=10μm. Note that the same result was obtained upon conditional activation of *puckered* 10hours after pupal formation using a gal80ts (not shown). **B:** Proportion of cell undergoing delamination outside the midline (top) and in the midline (bottom). Controls (*act<y<G4*) come from Fig. 1C,D. Error bars are 95% confidence intervals. P-values=Fisher exact test. **C:** z-projection of immunostained pupal nota expressing reporters of the transcriptional activity of Yki, *exp-lacZ* (top), and *diap1-lacZ* (bottom). The midline is in between the dotted lines (n=5 nota for each genotype).There is no downregulation of these targets in the midline, suggesting that Hippo pathway is not upregulated in the midline. Scale bars=10μm. **D:** z-projection of a live pupal notum expressing *kst::YFP* (βh-spectrin, under the control of the endogenous promoter, pseudo-colour, representative of 10 nota), a regulator of Hippo pathway sensitive to cell density[S2, S3]. Right graph shows the intensity profile along the grey square. There is no increase of Spectrin density in the midline, suggesting that Hippo pathway will not be upregulated by Spectrin in this region. The midline is in between the dotted lines. Scale bar=10μm. **E:** z-projection of E-cad::GFP in a live pupal notum with clones overexpressing Myc (purple). The midline is in between the dotted lines. Green spots are surviving cells and orange spots dying cells (or at least one daughter cell dying) after 700 minutes. Scale bar=10μm. There is a lot of cell death occurring also outside the midline region (compare with **Fig. 1C** control).

Supplemental experimental procedures

Fly stocks and clone induction

The following stocks were used in this study: *ubi-Ecad::GFP* (from [S4]), *ubi-Ecad::GFP; act-Gal4* (*act-gal4* on 3rd, Bloomington), *hs-flp22; ubi-Cad::GFP, UAS-mRFP; act<y+<Gal4* (gift from Legoff L), *ubi-Ecad::GFP,azot^{KO}* (recombinant, *azot* mutant from [S5]), *endo-Ecad::GFP* (knock-in,[41]), *hs-flp; endo-Ecad::GFP, tub-gal80^{ts}; act<y+<gal4, UAS-nlsRFP* (generated for this study), *UAS-diap1* (3rd, Bloomington), *UAS-p35* (2nd, Bloomington), *hs-flp;ubi-Ecad::GFP*; *ubi-nlsGFP FRT80B* (generated for this study, *ubi-nlsGFP FRT80B* from Bloomington), *Df3LH99 FRT80B* (gift from KangoSingh M), *dad-gal4* (Kyoto DGRC), *dad-RFP* (gift from Gonzalez-Gaitan M), *UAS-fwe RNAi* (2rd, VDRC), *UAS-apoliner* (on 2nd, Bloomington), *UAS-scat3* (on 2nd, gift of Miura M), *UAS-reaper; tub-gal80^{ts}* (*UAS-reaper* on X, Bloomington); *hs-flp22*; *act<y+<Gal4*, *UAS-GFP*; *fwe^{loseA}::mcherry* KI (*fwe^{loseA}::mcherry* KI from [S6]), *UAS-ras^{V12}* (on 3rd, Bloomington), *UAS-puc* (on 3rd, from Martin-Blanco E), *UAS-p53DN* (H159N, on 3rd, Bloomington), *exp-lacZ* and *diap1-lacZ* (respectively 2nd and 3rd, gift from Barry Thompson), *UAS-myc* (3rd, Bloomington), *kst::YFP* (*β_h-spectrin*, gift from Barry Thompson, DGRC 115-285).

All heat shocks were performed in a 37°C waterbath using glass tubes. For notum live imaging, all the clones were generated using a 9min heat shock, except for *Df3LH99 FRT80B* (Fig. 1C,D): two 1hour heat shocks with one hour of rest in between, Fig. 3A: 30min heat shock, Fig. 4: 20min heat shock and for the wing discs in Fig. S2C a 5min heat shock.

Immunohistochemistry

Dissection and immunostainings of nota were performed as indicated in[S7] with standard formaldehyde fixation and permeabilisation/washes in PBT 0.4% Triton. The following antibodies/markers were used: rat anti E-cad (DCAD2 concentrate, DSHB, 1/50), rabbit anti β-gal (1/200, Cappel). Dissected nota were mounted in Vectashield with DAPI (Vectorlab) and imaged on a Leica confocal SP2 using a 63X water immersion objective N.A. 1.3. Images shown are maximal z-projection containing adherens junction plane.

Pupal notum and wing disc live imaging, delamination analysis

Pupae were collected 48 or 72h after clone induction and dissected 16-18h after pupae formation (APF). Pupae were prepared as indicated in[S8] and imaged on a confocal spinning disc microscope (Till photonics) with a 40X oil objective (N.A. 1.35) or a point scanning confocal microscope Leica SP8 with a 63X objective (N.A. 1.4) using tile imaging (6 to 12 tiled positions) and Z-stacks (1 μm/slice) every 5min using autofocus at 25°C. Movies were performed in the nota close to the scutellum region containing the midline region. Movies shown are maximum projections after correction for bleach (using Fiji). Total duration was always 700min, except for Fig. 3C and Fig. 4 (1000min). For imaging of *UAS-rasV12* clones, the cross and the progeny were kept at 18°C, and the pupae were switched to 29°C 8 hours prior to the movie (to detect the clones with the RFP signal) and imaged at 29°C. The same procedure was used for induction of apoptosis by *UAS-reaper*, except that the 29°C switch was performed at the onset of the movie.

The midline region covers all the cells surrounded by the two most central lines of sensory organ precursors (SOP, located at the end of the movies). Every cell delamination event was localised manually inside and outside the midline and marked using Fiji. The probability of delamination was obtained by dividing the total number of delaminating cells in the movie by the initial number of cells (in the midline or outside the midline). The initial

number of cells was determined by segmenting the tissue at time 0 using Cell packing analyser[S9]. In the figures, cells were marked as dying cells if they died or if at least one of their daughter cell died before the end of the movie.

Wing-discs (Fig. S2C) were dissected in Schneider media 48h after clone induction and imaged in a drop of media in a glass bottom MaTek petri-dish using a point scanning confocal microscope Leica SP8 with a 63X objective (N.A. 1.4). Removal of the signal from the peripodal cells and selection of the *fwe^{loseA}::mcherry* signal from the junction plane were performed by using a Matlab macro for selective plane projection[S6].

Analysis of adult thorax

Width of the midline in the adult thorax was measured using adult female raised at 25°C (control: *dad-gal4*, versus *dad-gal4/UAS-diap1*). The midline was defined by region delimited by the two most central lines of bristles and the width was measured along a line connecting the two aDT macrochaetes. The width of the two adjacent lines of bristles was measured along the same line, and we plotted for each notum the log2 of the midline width divided by the mean of the two lateral line width.

Live imaging of caspase activation

Live imaging of caspase activation was performed on live pupal notum 16-18h after pupae formation on 10 hours movies using *act-gal4* driver crossed with *UAS-apoliner* or *UAS-scat3*.

For *apoliner*, we detected every delamination event looking at the membrane signal in the apical plane, and located the onset of relocalisation of the GFP signal to the nucleus to calculate the lag-time between caspase activation and cell delamination.

For *scat3*, imaging was performed on a point scanning confocal Leica SP8 using the 405 laser line for excitation and simultaneous detection of the CFP and the YFP signal. FRET signal was retrieved on Fiji by smoothing the signal (Gaussian blur, 1px width) and calculating the ratio of the YFP signal over the CFP signal. Delamination events were detected using the apical CFP signal and we manually found the corresponding onset of caspase activation to calculate the lag time.

Analysis of cell delamination

Cell delamination were randomly picked in the midline in *ubi-Ecad::GFP; act-gal4* and *ubi-Ecad::GFP; act-gal4* crossed with *UAS-diap1*. For induction of apoptosis, we crossed *ubi-Ecad::GFP; act-gal4* males with *UAS-reaper; tub-gal80ts* females. The cross and the progeny were kept at 18°C, and the pupae were eventually filmed in an incubator at 29°C (permissive temperature). Delamination events were selected outside the midline. Evolution of surface over time was measured manually on Fiji, normalised by the initial surface and plot against the number of vertices. The scatter plot in Fig. S1D correspond to the normalised area when cells have 4 vertices (which was used previously to distinguish D1 and D2 delamination types[S1])

Particle Image Velocimetry and tissue wounding

PIV was performed on MATLAB using the MatPIV toolbox (J.K. Sveen) as previously performed[S10]. PIV vector fields were obtained after reducing movies size by binning, and subdividing the picture in 64x64pixel windows for cross-correlation analysis with 50% overlap between windows. The final vector field is composed of displacement vectors separated by 32 pixels (15.5 μm). Vector fields were averaged in time using an averaging window of 9 frames centred on the current frame. PIV vector fields shown in the figures are the average of displacement over the total duration of the movies (700 to 1000min) representing a single notum. Convergence is defined as the opposite of the vector field divergence (calculated on Matlab). Convergence was calculated on every 32px x 32px square (15.5 μm, window containing 2 to 4 cells) and averaged over the total duration of the movie. Binning of the death probability plot against the local convergence was performed on an Igor pro homemade macro (Wavemetrics).

For analyse in Fig. S3C, we plot the local convergence over time and plot the delamination events occurring in the same window region. For each delamination event, the closest peak of convergence was automatically located on Matlab. The convergence function was smoothed in time (3 successive smooths with a 9 frames window), the derivative calculated, and points where derivative is null, second derivative<0 and convergence>0 counted as peak of convergence.

Wound healing was induced in *endo-Ecad::GFP* notum by long time exposure to a full power Argon laser on a point scanning confocal Leica SP8. A Region Of Interest (ROI, 100x600 px, 1px=0.10 μm) perpendicular to the midline (anterior to the aDC macrochaetes) was scanned at full power (using 405, 454, 488 and 514 laser lines) 1000 times. Movie was then recorded over 1000min. Delamination events were counted in the midline anterior and posterior to the wound, excluding a 20μm zone around the ROI (cells potentially directly damaged by laser

exposure and heat). For each notum, we calculated the proportion of delaminating cells (as indicated above) anterior and posterior to the wound, and plotted the log2 of the ratio. The same analysis was performed for *endo-Ecad::GFP* nota without wounding excluding also a fictive wounded zone from the analysis.

Density and cell area analysis

Density fold change was calculated by segmenting the tissue at time 0 and at the end of the movie using Packing analyser. For each window used for PIV, we calculated the initial number of cells (center of mass located inside the window) and the final number of cells in the window. Density fold change was calculated as followed: $(n_{final}-n_{initial})/n_{initial.}$ Binning of the data was performed on Igor pro software.

The evolution of cell area in time was calculated by measuring cell apical surface at time 0 using Fiji and manually tracking the cell and its progeny until the end of the movie. We then measured the cell surface at the end of the movie or the sum of the surface of its daughter cells. Final surface was set to 0 for dying cells and these were excluded for the calculation of the average fold change of cell area shown in Fig. 4D.

Statistics

All the error bars shown in the figures are Standard Errors of the Mean (s.e.m.) or 95% confidence interval. Statistical tests are Fisher exact tests (two sided) for comparison of proportions or Mann-Whitney non-parametric tests, or t-test (normality tested with a Shapiro-Wilk test). Correlation coefficients are Pearson correlation coefficients, significance was calculated using the t-value. No statistical methods were used to set sample size. Experiments were not randomized, and we did not analyse experiments blindly. Every experiment was performed at least 2 independent times.

Supplemental References

S1. Marinari, E., Mehonic, A., Curran, S., Gale, J., Duke, T., and Baum, B. (2012). Live-cell delamination counterbalances epithelial growth to limit tissue overcrowding. Nature *484*, 542-545.

S2. Fletcher, G.C., Elbediwy, A., Khanal, I., Ribeiro, P.S., Tapon, N., and Thompson, B.J. (2015). The Spectrin cytoskeleton regulates the Hippo signalling pathway. The EMBO journal *34*, 940-954.

S3. Wong, K.K., Li, W., An, Y., Duan, Y., Li, Z., Kang, Y., and Yan, Y. (2015). beta-Spectrin regulates the hippo signaling pathway and modulates the basal actin network. The Journal of biological chemistry *290*, 6397-6407.

S4. Oda, H., and Tsukita, S. (2001). Real-time imaging of cell-cell adherens junctions reveals that Drosophila mesoderm invagination begins with two phases of apical constriction of cells. Journal of cell science *114*, 493-501.

S5. Merino, M.M., Rhiner, C., Lopez-Gay, J.M., Buechel, D., Hauert, B., and Moreno, E. (2015). Elimination of unfit cells maintains tissue health and prolongs lifespan. Cell *160*, 461-476.

S6. Levayer, R., Hauert, B., and Moreno, E. (2015). Cell mixing induced by myc is required for competitive tissue invasion and destruction. Nature *524*, 476-480.

S7. Jauffred, B., and Bellaiche, Y. (2012). Analyzing frizzled signaling using fixed and live imaging of the asymmetric cell division of the Drosophila sensory organ precursor cell. Methods in molecular biology *839*, 19-25.

S8. Bellaiche, Y., Gho, M., Kaltschmidt, J.A., Brand, A.H., and Schweisguth, F. (2001). Frizzled regulates localization of cell-fate determinants and mitotic spindle rotation during asymmetric cell division. Nature cell biology *3*, 50-57.

S9. Aigouy, B., Farhadifar, R., Staple, D.B., Sagner, A., Roper, J.C., Julicher, F., and Eaton, S. (2010). Cell flow reorients the axis of planar polarity in the wing epithelium of Drosophila. Cell *142*, 773-786.

S10. Levayer, R., and Lecuit, T. (2013). Oscillation and polarity of E-cadherin asymmetries control actomyosin flow patterns during morphogenesis. Developmental cell *26*, 162-175.